Journal of Molecular Liquids 294 (2019) 111639

Contents lists available at ScienceDirect

Journal of Molecular Liquids

journal homepage: www.elsevier.com/locate/molliq

Extension of the SAFT-VR-Mie equation of state for adsorption

Harry Cárdenas, Erich A. Müller*

Department of Chemical Engineering, Imperial College London, South Kensington Campus, London SW7 2AZ, UK

ARTICLE INFO

Article history:
Received 31 May 2019
Received in revised form 13 August 2019
Accepted 24 August 2019
Available online 31 August 2019

Keywords:
Adsorption
Nanopores
SAFT
Molecular simulation

ABSTRACT

An empirical extension of the Statistical Associating Fluid Theory (SAFT-VR-Mie) is presented to take into account the effect of confinement of fluids within cylindrical nanopores. The modification of the equation of state retains the bulk phase limit presented in the original formulation and adds a term corresponding to the contribution to the Helmholtz energy of the confined fluid. The resulting expression employs the fluid-fluid parameters obtained from fitting bulk fluid behaviour and adds two additional adjustable parameters reflecting the strength of the solid-fluid energy and the range of the surface attraction. The capability of the theoretical model is showcased by fitting adsorption isotherms of methane and *n*−nonane on activated carbons; ethane, *n*−hexane and benzene on MCM-41, and methane and carbon dioxide on carbon surrogate models of shale rocks; providing for an accurate correlation of the data with parameters that are temperature-independent and robust. The physical nature of the underlying model allows it to be mapped to fluid-solid molecular models which can then be resolved employing classical molecular simulation methods, providing for an avenue into probing not only the adsorption behaviour but also the transport and interfacial properties.

1. Introduction

The modelling of confined fluids, where a fluid is in equilibrium with a porous matrix, is of ubiquitous importance for the design and optimisation of physical, chemical and biological systems [1]. An understanding of adsorption at the nanoscale is key to the development of new materials for environmental remediation (e.g. to separate contaminants from waste flows) [2,3], for enhanced oil recovery [4,5], or in the fabrication of membranes for separation processes [6], to name a few. However, the theoretical modelling of fluids under confinement has historically lagged behind that of the more common bulk-fluid description. One presumed reason is the inherent complexity of describing the heterogeneous fluid behaviour for those molecules in the region situated close to the solid wall.

From the many strategies available to describe the adsorption phenomena, a first group corresponds to semi-empirical models that provide a simple way to predict adsorption with low computational cost and simple mathematical expressions. Examples of semi-empirical models are the Langmuir [7], Freundlich [8], and Brunauer-Emmett-Teller (BET) models [9], amongst many others [10]. These models excel at correlating experimental data, but have little or no predictive capabilities. A second group of models is available with a more robust theoretical grounding and consequently a higher accuracy for predictions, using thermodynamic theory as a starting point. Within this group, those based on classical density functional theory (DFT) [11-16] are typical. These models are inherently difficult to implement, especially for complex fluids, and consequently have been poorly adopted by the community, in spite of being considered the "golden standard" [17]. In this context, a special mention is also made to the potential theory of adsorption [18-20]. Intermediate between those two extremes one finds modified equations of state (EoS) for the prediction of fluids under confinement [21-24].

In order to develop a molecular theory for adsorption, the use of an equation of state can provide accurate results with short calculation times. An equation of state can, in principle, be used as a reference to represent both the bulk phase properties and the main effects of confinement. An advantage here is that one can tap into a large body of research that over the past decades has been developed to provide for the prediction of thermophysical properties of bulk fluids [25]. A seminal example is the model presented by Travalloni et al. [26,27], who proposed an extension of cubic equations of state to model fluids under confinement inside a cylindrical pore, recently extended to spherical pores [28] and to include pore size distributions [29]. Despite the accuracy that these models can reach, cubic equations of state are ill-suited to represent the high-density regions of phase space and have only a loose link to the properties of the underlying molecular model. On the other hand, there is much to be gained if a molecular-based EoS is employed, where a well-defined Hamiltonian describes

* Corresponding author.
E-mail address: e.muller@imperial.ac.uk (E.A. Müller).

https://doi.org/10.1016/j.molliq.2019.111639
0167-7322/

the physics. One such EoS is the statistical associating fluid theory (SAFT) [30,31], which has been successfully used to calculate the phase behaviour of complex fluid systems [32,33]. One of the first attempts to use the SAFT equation of state for adsorption calculation is the model proposed by Martinez et al. [34], where a theoretical model based on the SAFT EoS using a quasi-two-dimensional approximation was developed to describe the properties of adsorbed fluids. Kern and Johannsen [35] extended this two-dimensional model applying it to model the adsorption of methanol from supercritical carbon dioxide on an energetically heterogeneous adsorbent. Another SAFT-related work is the one from Franco et al. [36], who developed an implicit inhomogeneous model that can be added to a SAFT equation of state to calculate adsorption isotherms based on the mean value theorem.

In complement to the above-mentioned theories, the effects of confinement on fluid phase behaviour have been thoroughly studied using molecular simulations [37-40]. In general, the data obtained from molecular simulations can be employed as pseudo-experimental data to develop or improve models, however very few models have taken advantage of this to link directly EoS to simulation data. Barbosa et al. [41] used Monte Carlo simulations to evaluate geometric and energetic effects of different degrees of confinement on the fluid structure to modify the model proposed by Travalloni et al. [27]. Another example is given by Kong and Adidharma [42], where they used a model based on generalised van der Waals partition function and then compared it with Monte Carlo simulation data to test the accuracy of the model.

In this work, our goal is to develop an empirical expression from molecular simulation data that can be coupled to the statistical associating fluid theory, in its SAFT-VR-Mie version [43], for the prediction of adsorption isotherms. Grand Canonical Monte Carlo (GCMC) simulations of fluids adsorbed into cylindrical attractive pores are employed here as pseudo-experimental data to provide the benchmark data to interpret the theory in terms of the underlying molecular model.

2. Theoretical model

2.1. Generalised van der Waals theory for confined fluids

The proposed model starts from the fact that all the properties of a fluid can be obtained from the partition function, which for a canonical ensemble can be written as [44]:

$$Q(N,V,T)=\frac{1}{\lambda^{3N}N!}\int \exp\left(-\frac{\mathcal{V}(\mathbf{r}^N)}{kT}\right)d\mathbf{r}^N=\frac{1}{\lambda^{3N}N!}Z(N,V,T) \tag{1}$$

where N is the total number of particles, V is the volume, T is the absolute temperature, λ is the de Broglie thermal wavelength, $\mathcal{V}(\mathbf{r}^N)$ is the potential energy of the system, which itself is a function of the position of the particles ($\mathbf{r}^N$), k is the Boltzmann constant and Z is defined as the configurational integral. Despite Eq. (1) and the subsequent equations are written in terms of pure fluids, they can be easily extended for multicomponent mixtures.

In a realistic system, the dimensionality of the configurational integral conspires against any attempt to solve it explicitly. Hence, one must resort to approximations and simplifications to obtain estimates of its values. Defining the configurational canonical energy as the difference between the energy of a real gas and that of the ideal gas, it is possible to express it in terms of the configurational integral as [45]:

$$E_{\text{conf}}(N,V,T)=E(N,V,T)-E^{\text{IG}}(N,V,T)=kT^2\frac{\partial \ln Z(N,V,T)}{\partial T} \tag{2}$$

By integrating the previous equation, an expression for the configurational integral can be obtained as a function of the configurational energy. The lower integration limit will be the ideal gas case, while the upper limit will be the real fluid case. For the ideal gas, we assume that when the temperature in the system is high enough ($T\to\infty$), the fluid will behave as an ideal gas. The configurational integral of an ideal gas is basically a volumetric integral which leads to the definition of a free volume, V_f. The canonical partition function can then be rewritten as:

$$Q(N,V,T)=\left(\frac{q_{\text{int}}^N}{\lambda^{3N}N!}\right)V_f^N\exp\left(\int_\infty^T\frac{E_{\text{conf}}}{kT^2}dT\right) \tag{3}$$

where q_{int} is defined as the internal partition function, which considers the rotational, vibrational and electronic states for each particle [45,44].

If a solid attractive wall is added to the system, then two zones can be observed in the fluid; a bulk phase (homogeneous) and an adsorbed phase (heterogeneous). In this description, the interfacial region is ascribed to the adsorbed phase. In order to describe these two regions, the configurational energy for the fluid can be split into two contributions, leading to the following expression for the canonical partition function for adsorption:

$$Q_{\text{ads}}(N,V,T)=\left(\frac{q_{\text{int}}^N}{\lambda^{3N}N!}\right)V_f^N\exp\left(\int_\infty^T\frac{E_{\text{conf,mol-mol}}}{kT^2}dT\right)\times\exp\left(\int_\infty^T\frac{E_{\text{conf,mol-wall}}}{kT^2}dT\right) \tag{4}$$

where $E_{\text{conf,mol-mol}}$ is the configurational energy due to molecule-molecule interactions, and $E_{\text{conf,mol-wall}}$ is the configurational energy due to the interaction between the fluid and the solid wall.

SAFT equations of state for bulk fluids can be written as a perturbation sum of different Helmholtz free energy contributions. The following thermodynamic expression relates the canonical partition function in terms of the Helmholtz free energy [46]:

$$A(N,V,T)=-kT\ln Q(N,V,T) \tag{5}$$

The first three terms of the RHS of Eq. (4) correspond to the bulk phase, so then can be directly expressed in terms of the Helmholtz free energy;

$$Q_{\text{ads}}(N,V,T)=\exp\left(-\frac{A_{\text{bulk}}(N,V,T)}{kT}\right)\exp\left(\int_\infty^T\frac{E_{\text{conf,mol-wall}}}{kT^2}dT\right) \tag{6}$$

If one defines the contribution to the Helmholtz free energy due to the fluid-solid interactions for adsorption as;

$$\frac{A_{\text{ads}}(N,V,T)}{kT}=-\int_\infty^T\frac{E_{\text{conf,mol-wall}}}{kT^2}dT \tag{7}$$

Then, the canonical partition function for confined fluids can be uniquely written as a sequence of terms contributing to the total Helmholtz free energy. The bulk contribution for the Helmholtz free energy can be obtained from the SAFT equation of state, which can be broken down into three contributions: ideal gas, monomer, and chain (neglecting the association term). In summary, the canonical partition function can be conveniently expressed in terms of a sum of well-defined contributions;

$$\ln Q_{\text{ads}}(N,V,T)=-\frac{1}{kT}\left(A_{\text{ideal}}+A_{\text{mono}}+A_{\text{chain}}+A_{\text{ads}}\right) \tag{8}$$

where the last term, A_{ads}, corresponds to the effect of the adsorbed region, where the fluid-solid interactions are dominant.

2.2. Model description

The expression for the adsorbed region contribution, as was shown in Eq. (7), depends on the energy that accounts for the interactions between the solid wall and the particles close enough to feel the influence of the wall.

The model used here is based on the work of Travalloni et al. (2010) [26], where the fluid is adsorbed into a cylindrical pore and the interaction between the fluid particles and the solid wall is described following the Square-Well (SW) potential:

$$u_{\text{mol-wall}}(r) = \begin{cases} +\infty & \text{if } r \geq r_p - \frac{\sigma}{2} \\ -\epsilon_w & \text{if } r_p - \frac{\sigma}{2} - \delta_w \leq r < r_p - \frac{\sigma}{2} \\ 0 & \text{if } r > r_p - \frac{\sigma}{2} - \delta_w \end{cases} \tag{9}$$

where r_p is the pore radius, ϵ_w is the potential depth of the molecule-wall interaction (energetic parameter), and δ_w is the width of the range for the SW potential. The distance r is the radial position of the centre of mass of the molecule with respect to the central axis of the pore.

The cylindrical pore has three different regions displayed in Fig. 1: the first zone (A) corresponds to the bulk phase, where only fluid-fluid interactions come into play, the second zone (B) is the adsorbed region, where both fluid-fluid and fluid-solid interactions have to be considered, and the third zone (C) is an empty volume due to the mutual exclusion between a hard wall and a hard sphere ($\sigma/2$).

2.3. The statistical associating fluid theory (SAFT)

2.3.1. The bulk fluid

The version of the statistical associating fluid theory (SAFT) used in this work corresponds to a particular case of the generic SAFT methodology for potentials of variable range for molecules conformed of segments interacting through the Mie potential [47], u_{Mie}, which can be expressed by;

$$u_{\text{Mie}}(r) = \frac{\lambda_r}{\lambda_r - \lambda_a}\left(\frac{\lambda_r}{\lambda_a}\right)^{\frac{\lambda_a}{\lambda_r - \lambda_a}} \epsilon \left[\left(\frac{\sigma}{r}\right)^{\lambda_r} - \left(\frac{\sigma}{r}\right)^{\lambda_a}\right] \tag{10}$$

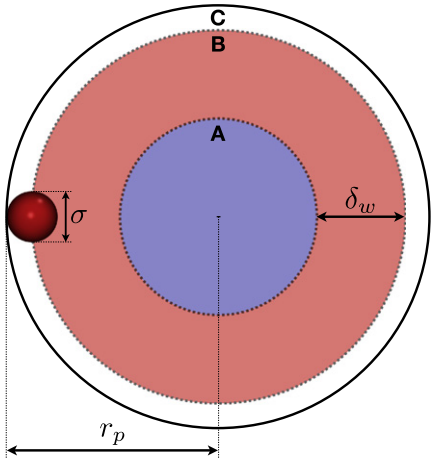

Fig. 1. Model assumed for the cylindrical pore in this work. In region A (bulk) only fluid-fluid interactions are relevant. In region B (adsorbed) both fluid-fluid and fluid-wall interactions are relevant. Region C is an excluded volume.

where λ_r and λ_a are the repulsion and attraction parameters of the intermolecular potential, respectively, r is the centre-to-centre distance of the interacting segments, ϵ is the energy scale corresponding to the potential well depth for the fluid-fluid interactions, and σ is the length scale corresponding with an effective segment diameter.

The homogeneous Helmholtz free energy density of SAFT-VR-Mie EoS for non-associating chain fluids is given by [43];

$$a = a^{\text{ideal}} + a^{\text{mono}} + a^{\text{chain}} \tag{11}$$

where $a = A/(NkT)$, A is the total Helmholtz free energy, N is the total number of molecules in the system, and T is the temperature of the system. The term a^{ideal} represents the ideal gas Helmholtz free energy, a^{mono} is the Helmholtz free energy of unbounded monomer contribution for a chain formed of m_s tangential segments, and a^{chain} is the Helmholtz energy due to the formation of chain molecules [43].

The other thermodynamic properties can be obtained from the Helmholtz free energy following standard thermodynamic relationships. The pressure is obtained from the partial derivative with respect to the volume, $P = -(\partial A/\partial V)_{N,T}$, and the chemical potential from the partial derivative with respect to the number of particles, $\mu = (\partial A/\partial N)_{T,V}$ [43].

The contribution to the Helmholtz free energy due to the dispersion forces amongst the monomers, considering that m_s monomers conform each molecular chain is given by;

$$a^{\text{mono}} = m_s a^{\text{M}} = m_s\left(a^{\text{HS}} + \beta a_1 + \beta^2 a_2 + \beta^3 a_3\right) \tag{12}$$

where a^{M} is the excess Helmholtz free energy density per each monomer bead, and it can be expressed as a series expansion with respect to the inverse of the temperature, $\beta = 1/kT$, and truncated to the third term. This expansion starts with a^{HS}, which corresponds to the Helmholtz free energy related with a fluid modelled as a hard sphere (HS), while the rest of the contributions (a_1, a_2 and a_3) are the first three perturbation terms associated with the attractive energy [43].

The chain contribution comes from linking the monomeric segments together in order to form the chain molecule. This expression is given in terms of the contact value of the pair distribution function of the monomers, $y^M(\sigma)$;

$$a^{\text{chain}} = (1 - m_s)\ln y^M(\sigma) \tag{13}$$

The monomer-monomer correlation function is evaluated at hard-core contact, which means that the centre-centre distance between the monomers is the molecular diameter of the monomer. This correlation can be obtained from the high-temperature expansion of the pair radial distribution function, $g^M(\sigma)$ and from the intermolecular potential $u(r)$, in the following expression;

$$y^M(r) = \exp\left[\beta u(r)\right] g^M(r) \tag{14}$$

The high-temperature expansion of the pair radial distribution function uses the hard-sphere (HS) reference to start a series expansion truncated to the second order contribution of the radial distribution function.

For details with respect to the evaluation of the different contributions, the reader is referred to ref. [43] and [48].

2.3.2. The confined fluid

When a fluid is under confinement, besides the attraction from the solid wall, the distribution of particles will be affected depending

on the shape of the pore. The coordination number is a measure of short-range order in fluids, and it is defined as the number of molecules that a central particle holds as its closest neighbours in a system. For the bulk fluid phase case, this coordination number can be approximated to 10, which means that every particle in average is surrounded by 10 molecules [49]. The confinement in a cylindrical pore will affect the coordination number, because the number of neighbours for a certain particle will be now a function of the pore dimension. For the case of a cylindrical pore with radius $\sigma/2$ for the maximum confinement case, in the radial direction only one molecule can be placed in the pore, and this particle will have only two neighbours: one in the $+z$ direction and another one in the $-z$ direction, leading to a coordination number of 2 [26]. A linear relation can be used in order to satisfy both limits: the bulk case, for big pores ($r_p \to \infty$) where the coordination number is 10, and the maximum confinement case, where the coordination number is 2.

This reduction in the coordination number affects directly the attractive energy, which in SAFT corresponds to the first three perturbation terms in the monomer contribution, so one must scale this term to consider the effects of confinement;

$$a^{\text{mono}}_{\text{confinement}} = m_s a^{M}_{\text{confinement}} = m_s \left(a^{HS} + \left[1 - \frac{2}{5}\frac{\sigma}{r_p} \right] \left(\beta a_1 + \beta^2 a_2 + \beta^3 a_3 \right) \right) \tag{15}$$

From Eq. (15) it is possible to observe that both limits in the coordination number are satisfied by the term inside the square brackets. First, for a big pore radius this term takes the value of 1 leading to the bulk phase monomer term. On the other hand, for the smallest pore radius ($\sigma/2$) this term will be 1/5, a value that agrees with maximum confinement condition where each molecule has only two neighbours.

Considering that the chain term is the contribution of bonding the monomeric segments together to form a chain, we do not have to modify this term for confinement because the correction is already included in the monomer term.

2.3.3. Adsorption contribution (A_{ads})

The configurational energy definition is based on the pairwise additivity for the attractive part of the molecule-molecule interaction potential [45]:

$$E_{\text{conf}}(N, V, T) = \frac{N^2}{2V} \int u(r) g(r; \rho, T) d\mathbf{r} \tag{16}$$

where $u(r)$ is the intermolecular potential and $g(r; \rho, T)$ is the pair correlation function for a fluid composed of molecules interacting with the potential $u(r)$. To calculate the configurational energy for the case of a solid wall interacting with particles from a fluid phase, the pre-factor of the Eq. (16) is reduced to N/V because the interactions are between the surface and the molecules. Formally, one would require to solve Eq. (16) with the knowledge of the inhomogeneous density distribution, which of course is the desired "answer". More sophisticated treatments, based on Density Functional Theory would directly solve for this quantity. Here, however, in the spirit of producing a simple closed-form expression for simple fluids, the radial distribution function can be approximated to a constant value equal to 1 (mean field approximation). The configurational energy for fluid-solid interaction can then be expressed as [26]:

$$E_{\text{conf,mol-wall}} = -N_p \epsilon_w = -N F_p \epsilon_w \tag{17}$$

where N_p is the number of particles in the adsorbed zone, and N is the total number of particles in the system. The exact number of molecules interacting with the pore wall, N_p, is the key quantity to calculate. The term F_p is defined as the fraction of confined molecules that occupies the adsorbed zone in the pore (Square-Well region).

The maximum molecular density, $\rho_{\max}$, that is used to reduce the density, is a function that depends on the molecular size, but also on the pore dimensions (the radius r_p). This density considers the formation of a structured layer of hard spheres close to the wall, and by using analytical and experimental data of mean porosity of loosely packed beds [50] the following expression can be used to express this density [26];

$$\rho_{\max}\sigma^3 = 0.86486 \frac{6}{\pi} \left(1 - c_1 - c_2 \exp\left(c_3 \left(0.5 - \frac{r_p}{\sigma} \right) \right) + c_4 \exp\left(c_5 \left(0.5 - \frac{r_p}{\sigma} \right) \right) \right) \tag{18}$$

where $c_1 = 0.393684$, $c_2 = 0.250942$, $c_3 = 0.620861$, $c_4 = 0.311601$, and $c_5 = 4.01377$ are fitting parameters obtained by adjusting the values of porosity as a function of the pore radius [26]. This maximum density is for a close-packed fluid, however this condition is not reached at vapour-liquid equilibrium conditions, so a pre-factor is included (the value 0.8648 in Eq. (18)). This pre-factor comes from the ratio between the limits on the packing fractions for a glass and a crystal structure [51], assuming that the maximum condition approachable inside a pore will be closer to a glass rather than a crystal.

The model proposed in this work considers two important limits for the fraction of confined molecules in the adsorbed region, F_p. On the first hand, when the system has low temperature and low density ($T \to 0$ and $\rho \to 0$) all the particles inside the pore will be inside the SW (adsorbed) region, hence the $F_p = 1$. On the other hand, for a system with high density and/or high temperature ($T \to \infty$ and $\rho \to \rho_{\max}$), the pore will be saturated with liquid, so the order of the particles inside will follow a random distribution. This random particle distribution is purely geometric, so it can be obtained by applying probability rules over the cylindrical volume. This random distribution is the ratio between the available volume for adsorption and the total volume of the cylinder;

$$F_{pr} = \frac{r_p^2 - (r_p - \sigma/2 - \delta_w)^2}{r_p^2} \tag{19}$$

The empirical expression for the particle distribution inside a cylindrical pore, F_p, proposed here is a modification of the one presented by Travalloni et al.(2010) [26], in order to improve the link between the simulation results and the model (Fig. 2):

$$F_p = F_{pr} + (1 - F_{pr})(1 - a_p \exp(-\Psi)) \left(1 - \left(\frac{\rho}{\rho_{\max}} \right)^{b_p + c_p \Psi} \right)^{\theta} \tag{20}$$

where θ is called the confinement degree, $\theta = r_p/(\delta_w + \sigma/2)$ [26], and $\Psi = d_p \epsilon_w/(kT)$ is a characteristic energy scale. The confinement degree is a geometric term that reflects the ratio of the bulk phase region compared with the SW region, and it allows to modify the shape of F_p for different levels of confinement. For large pore radius, the random distribution, F_{pr}, is preferred because the effect of the fluid-wall interactions is smaller [26]. The other terms presented; a_p, b_p, and c_p are empirical functions of the pore size, while d_p is a function of the number of segments, m_s, and the ratio of potential

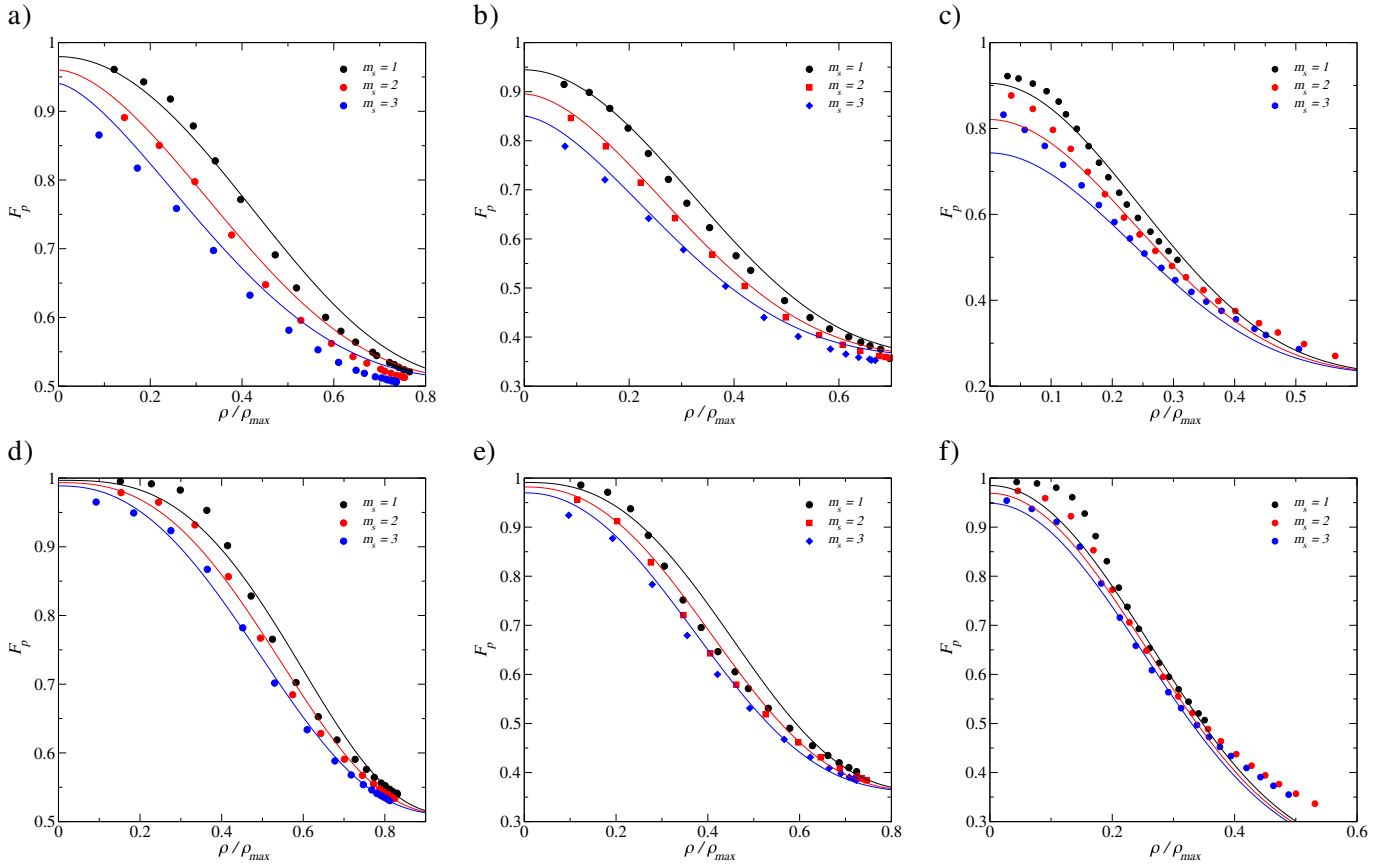

Fig. 2. Particle distribution, F_p, as a function of the reduced density, $\rho/\rho_{\max}$. Solid circles are GCMC simulation results, and solid lines correspond to Eq. (20), for different pore sizes, fluid-solid energy interactions and number of segments, m_s. The temperature is 98.5 K for $m_s = 1$, 133.4 K for $m_s = 2$ and 156.9 K for $m_s = 3$. The SW width was kept constant as $\delta_w = 0.5\sigma$. a) $r_p = 3.33\sigma$ and $\epsilon_w/k = 400$ K, b) $r_p = 5.0\sigma$ and $\epsilon_w/k = 400$ K, c) $r_p = 8.33\sigma$ and $\epsilon_w/k = 400$ K, d) $r_p = 3.33\sigma$ and $\epsilon_w/k = 600$ K, e) $r_p = 5.0\sigma$ and $\epsilon_w/k = 600$ K, and f) $r_p = 8.33\sigma$ and $\epsilon_w/k = 600$ K.

depths, ϵ_w/ϵ, between the fluid-solid interactions and the fluid-fluid interactions:

$$a_p = 0.7464 + \left(0.58558\frac{r_p}{\sigma}\right) - \left(0.01258\left(\frac{r_p}{\sigma}\right)^2\right) \tag{21}$$

$$b_p = 1.958234 - \frac{2.152195}{1 + \left(0.18989\frac{r_p}{\sigma}\right)^{5.5209}} \tag{22}$$

$$c_p = -0.030413 + \frac{0.522083}{1 + \left(0.177613\frac{r_p}{\sigma}\right)^{4.72}} \tag{23}$$

$$d_p = 1 + (m_s - 1)\frac{0.06}{m_s}\frac{\epsilon_w}{\epsilon} \tag{24}$$

The functions a_p, b_p, c_p and d_p, are fitted from Grand Canonical Monte Carlo simulation data (detailed in the next section) for different pore sizes, Square-Well widths and wall-fluid energy interactions using Lennard-Jones fluids with three different chain lengths. By using Eq. (20), the particle distribution can be expressed as a function of the density of the system.

The final form of the adsorption contribution to the Helmholtz free energy density can be expressed as;

$$\begin{aligned} a^{\text{ADS}} &= \frac{A_{\text{ads}}}{NkT} \\ &= -\frac{\epsilon_w}{k}\left[\frac{F_{pr}}{T} + (1 - F_{pr})\int_T^\infty \frac{1}{T^2}\left(1 - a_p \exp\left(-\Psi\right)\right)\right. \\ &\quad \left.\times\left(1 - \left(\frac{\rho}{\rho_{\max}}\right)^{b_p + c_p\Psi}\right)^\theta dT\right] \end{aligned} \tag{25}$$

In the previous equation, the integral from T to ∞ has to be calculated numerically.

2.4. Molecular simulations

2.4.1. Simulation details

We have used Grand Canonical Monte Carlo (GCMC) simulations [52] to study the particle distribution inside cylindrical pores. The system consists of a cylinder with periodic boundary conditions in the axial coordinate. The pore has an attractive wall where the fluid-solid interactions are taken to conform to the Square-Well potential (Eq. (9)). Considering that the proposed model uses the SAFT equation of state to model the fluid-fluid interactions, in the simulations these interactions are modelled using the Mie potential

displayed in Eq. (10). All the systems were allowed to equilibrate for 5×10^6 configurations and the number of particles adsorbed in the pores were sampled for another 5×10^6 configurations. In order to calculate the distribution inside the cylindrical pore, the number of particles in the Square-Well region was recorded for each configuration so the ratio between the particles in this region and the total number of particles inserted will give the value of F_p. In GCMC simulations, translation, insertion and deletion of particles are carried out, and each type of move is chosen with equal random probability. In this ensemble, the chemical potential (μ) is specified instead of the pressure. Considering that the adsorption isotherms are expressed as the adsorbed amount as a function of the pressure, a relation between both the pressure and the chemical potential is employed. The same chemical potential is used for simulations in the confined space and in the bulk phase, where from the latter is possible to obtain the bulk fluid density related to a specific chemical potential. In order to obtain the pressure of the system, molecular dynamics simulations in the canonical ensemble (N, V, T) were performed using GROMACS 5.1 simulation open source suite [53], using the temperature and density from GCMC simulations of the bulk phase.

2.4.2. Validation with molecular simulations: adsorption of a LJ fluid on a cylindrical nanopore

The theoretical model on its own is built upon a well-defined molecular description of both the fluid and the solid. As such, one could perform molecular simulations to directly probe the approximations in the theory. There is, unfortunately, an incongruity between the fluid model described as a continuous soft-sphere Mie model and the surfaces, described with Square-Well interactions. This mis-alignment has the consequence that when describing the solid-fluid interactions within a simulation both models become incompatible, i.e. a particle would exhibit smoothly decaying interactions between the fluid particles but sharp impulse-like forces when encountering walls and/or the boundary of the SW range. This mismatch will be particularly important if molecular dynamics were used to probe the confined fluid behaviour.

We encounter the above problem when attempting to use simulations to test the theory. In order to provide for a realistic model we have employed a Mie potential to characterise the fluid-solid interactions in our molecular simulations. Ideally, one might be able to map two different pairwise potential invoking their conformal behaviour. This has been done for bulk fluids SW and the hard core + Yukawa tail (HCY) spheres [54] and between the hard sphere and the LJ fluid [55] by comparing and matching their macroscopic thermodynamic properties. A similar conformal analysis of the Mie fluid also shows that there is a mapping between different sets of (λ_r, λ_a) pairs [56]. Notwithstanding, for fluid-surface potentials, there is no accepted procedure for mapping potentials. As in the bulk phase, one could attempt to match the form of the potential or otherwise the free energy profile [57]. In our models, we have employed a Mie $(\lambda, 3)$ potential, i.e. Eq. (10) where the attractive potential is fixed to 3 and the repulsive potential is varied. This choice mimics the result of the implicit integration of a surface composed of Mie particles with an attractive exponent of 6, an expected value accounting for simple dispersion [58,59].

To validate the proposed model, GCMC simulations were used as a benchmark. The adsorption of a single Lennard-Jones (LJ) bead fluid inside a cylindrical nanopore at a subcritical condition was studied. The cylindrical pore has an implicit attractive wall, and the fluid-solid interactions follow a Mie-3 potential, where the repulsive exponent is variable and the attractive one is fixed as 3. This potential is then effectively mapped onto a SW potential.

Although all the results can be normalised, for simplicity we express them in absolute units. The model fluid is a single sphere with a molecular diameter of 0.3 nm, a potential depth of $\epsilon/k = 100$ K, a repulsive exponent of 12 and an attractive exponent of 6. The adsorption isotherms were calculated at the temperature of 100 K ($\epsilon/kT = 1$) to ensure a sub-critical condition.

The value of surface energy parameter for the simulations, $\epsilon_{w,\mathrm{sim}}$, is left as an adjustable parameter to match the corresponding energy of the original surface SW model, $\epsilon_{w,\mathrm{model}}$. Fig. 3 shows how the theoretical model can reproduce the simulation results for two different values of fluid-solid energy interaction and three different potential ranges. The left-hand graph, Fig. 3-a, corresponds to a lower fluid-solid interaction: for the simulations we use the value of $\epsilon_{w,\mathrm{sim}}/k = 500$ K, while for the model the energy is $\epsilon_{w,\mathrm{model}}/k = 350$ K. On the right-hand graph, Fig. 3-b, the fluid-solid interaction is stronger: for the simulations the value of $\epsilon_{w,\mathrm{sim}}/k = 750$ K matches the model energy of $\epsilon_{w,\mathrm{model}}/k = 520$ K. Both graphs in Fig. 3 present three different adsorbed region widths (blue > red > black). For the simulations, the width of the adsorbed region is represented by the repulsive exponent, λ_w, and the values in descending order are; 3.2, 5.5, 40. The corresponding SW widths for the theory are; 1.75σ, 1.0σ and 0.5σ, respectively. Following the

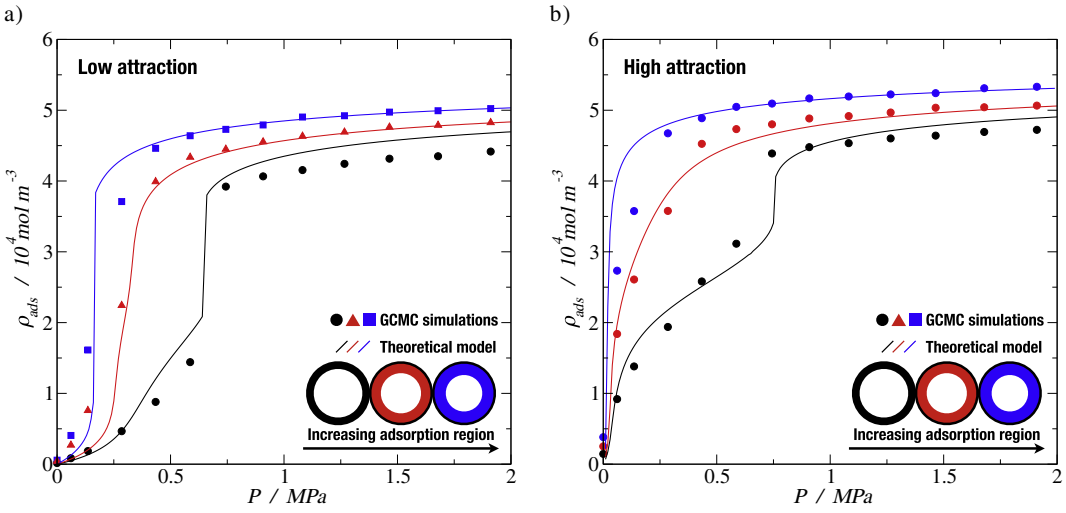

Fig. 3. GCMC simulation results for the adsorption of a LJ fluid into a cylindrical pore of $r_p = 1.5$ nm at 100 K. Fluid-solid energy interaction of: a) $\epsilon_{w,\mathrm{sim}}/k = 500$ K and $\epsilon_{w,\mathrm{model}}/k = 350$ K, b) $\epsilon_{w,\mathrm{sim}}/k = 750$ K and $\epsilon_{w,\mathrm{model}}/k = 520$ K. Solid symbols are simulation results: black circles are for $\lambda_w = 40$, red triangles are for $\lambda_w = 5.5$, and blue squares are for $\lambda_w = 3.2$. Solid lines correspond to the proposed model: black for $\delta_w = 0.5\sigma$, red for $\delta_w = 1.0\sigma$, and red for $\delta_w = 1.75\sigma$.

IUPAC classification [60,17], it is seen that the proposed model can predict multiple types of adsorption isotherms, such as type I (blue and red lines in Fig. 3-b), type III (blue and black lines in 3-a), type IV (black line in 3-b) and type V (red line in 3-a).

2.5. Equilibria calculations

To obtain the adsorbed amount in the equilibrium, the criteria to satisfy is the equality of temperature and chemical potential in both bulk and adsorbed phases:

$$T_{\text{bulk}} = T_{\text{ads}} \tag{26a}$$

$$\mu_{\text{bulk}}(T, \rho_{\text{bulk}}) = \mu_{\text{ads}}(T, \rho_{\text{ads}}; r_p, \delta_w, \epsilon_w) \tag{26b}$$

where μ_{bulk} is the chemical potential of the bulk phase and μ_{ads} is the chemical potential of the adsorbed phase. The former is a function of the temperature of the system, the bulk density and the molecular parameters for the fluid particles, while the latter is a function of the temperature, the adsorbed density, the molecular parameters of the fluid particles, the radius of the pore r_p, the energy of the fluid-solid interaction ϵ_w, and the Square-Well width δ_w. The bulk phase chemical potential can be obtained directly from SAFT by differentiating the Helmholtz free energy, $\mu_{\text{bulk}} = (\partial A/\partial N)_{T,V}$ [43]. The adsorbed phase chemical potential can be obtained from $\mu_{\text{ads}} = -kT(\partial \ln Q_{\text{ads}}/\partial N)_{T,V}$, where $\ln Q_{\text{ads}}$ can be obtained in a similar fashion from Eq. (8), leading to;

$$\mu_{\text{ads}} = \left(\frac{\partial \left(A_{\text{ideal}} + A_{\text{mono,conf.}} + A_{\text{chain}} + A_{\text{ads}} \right)}{\partial N} \right)_{T,V} \tag{27}$$

where $A_{\text{mono,conf}}$ corresponds to the monomer contribution to the Helmholtz free energy with the modification for confinement according to Eq. (15). A_{ads} is the Helmholtz free energy for the inhomogeneous fluid close to the wall, which is obtained from Eq. (25). Both parameters characterising the fluid-solid interaction: the potential range δ_w and the potential depth ϵ_w, are in principle unknown and have to be fitted to experimental data.

3. Results

We present in this section the application of the proposed model to selected experimental data.

3.1. Methane and n−nonane on activated carbon

In order to assess the performance of the proposed model with experimental adsorption data for carbons, we study the adsorption of pure methane and pure n−nonane. In spite that activated carbon is expected to be dominated by slit-like geometries, one observes that the cylindrical pore model has enough flexibility to correlate these data.

The adsorption of pure methane on activated carbon JX-101 at three different temperatures [65] is first presented. For the activated carbon JX-101 a surface area of 1500 m^2/g, a micropore volume of 0.5 mL/g and a total pore volume of 0.52 mL/g are reported, which suggests to a pore size of 0.63 nm. For the molecular model, the pore size is larger than the one reported from the experiments due to the finite size of the particles. The effective pore radius for the model is taken as the experimental value plus half of the molecular diameter ($\sigma/2$). The molecule of methane was modelled as a single bead, and the molecular parameters are reported in Table 1 [61].

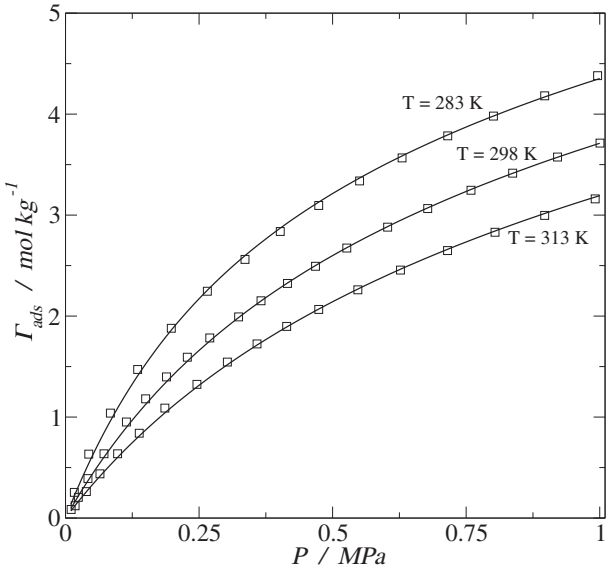

Fig. 4. Adsorption of methane on activated carbon at different temperatures. Open squares are experimental data [65] and solid lines represent the model proposed in this work.

There are three different reported temperature values for the adsorption of methane on activated carbon; 283 K, 298 K and 313 K. The model proposed was tested to correlate these experimental data sets by fitting the fluid-solid energy interaction, ϵ_w, and the adsorbed region width, δ_w. Fig. 4 displays the model fit of the adsorption isotherms for pure methane at the three different temperatures mentioned.

The values of potential depth, ϵ_w, seem to be temperature dependent, increasing slightly their value as the temperature decreases. The adsorbed region width values are kept constant for the different temperature values. An excellent agreement can be seen between the experimental data and the model from this work.

The second set of data corresponds to the adsorption of n−nonane on activated carbon BAX950 at three different temperatures; 303 K, 313 K and 323 K [66]. Here, the n−nonane molecule is modelled as 3 tangential segments within a fully flexible chain, and the parameters for the fluid-fluid interactions are reported in Table 1 [62]. From the experimental data we know that the pore volume is 0.89 cm^3/g, and that the pore has an extensive meso- and macroporous structure in addition to a microporous structure (Table 2). From fitting the experimental data with the proposed model it was possible to find that the equivalent pore radius for this data set is 2.2 nm, where other parameters for the fluid-solid interactions can be found in Table 3.

Table 1
Parameters for the SAFT-VR Mie EoS used for the fluid-fluid interactions.

Component	m_s	σ / nm	ϵ/k / K	λ_r	λ_a
Methane [61]	1	0.3736	151.45	12.32	6
Ethane [62]	1	0.4349	330.25	27.30	6
Carbon dioxide [63]	1	0.3741	353.55	23.00	6.66
n−Hexane [62]	2	0.4508	376.35	19.57	6
Benzene [62]	2	0.3978	353.93	14.23	6
Benzene (ring) [64]	3	0.3441	230.30	10.45	6
n−Nonane [62]	3	0.4406	374.21	18.31	6

Table 2
Parameters for the adsorption of methane on activated carbon JX-101. σ corresponds to the molecular diameter of the fluid.

T / K	ϵ_w/k / K	δ_w/σ
283	1208	0.2
298	1190	0.2
313	1180	0.2

Table 3
Parameters for the adsorption of $n-$nonane on activated carbon BAX950.

T / K	ϵ_w/k / K	δ_w/σ
303	3755	0.86
313	3748	0.86
323	3741	0.86

Fig. 5 displays the model fit to the adsorption isotherms of pure $n-$nonane on activated carbon at 303 K, 313 K and 323 K. The empty symbols correspond to the experimental data, while the solid lines are the model from this work for different temperatures. The adsorption data was fit accurately exhibiting type I isotherms.

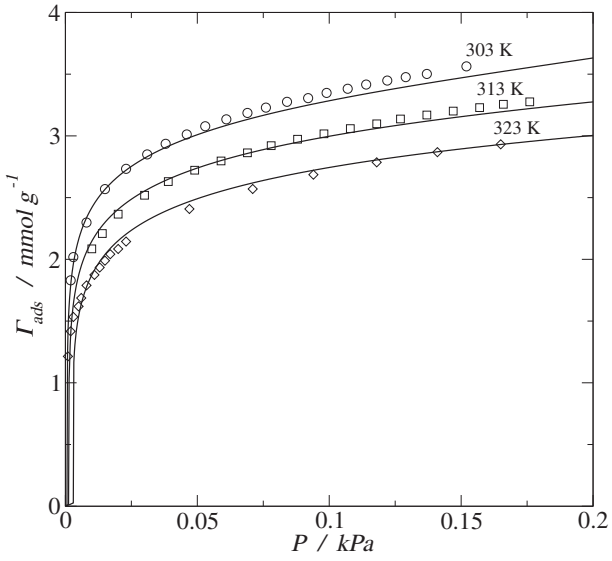

Fig. 5. Adsorption of $n-$nonane on activated carbon BAX950 at three different temperatures; 303 K, 313 K and 313 K. Open symbols are experimental data [66] and the solid lines are the proposed model.

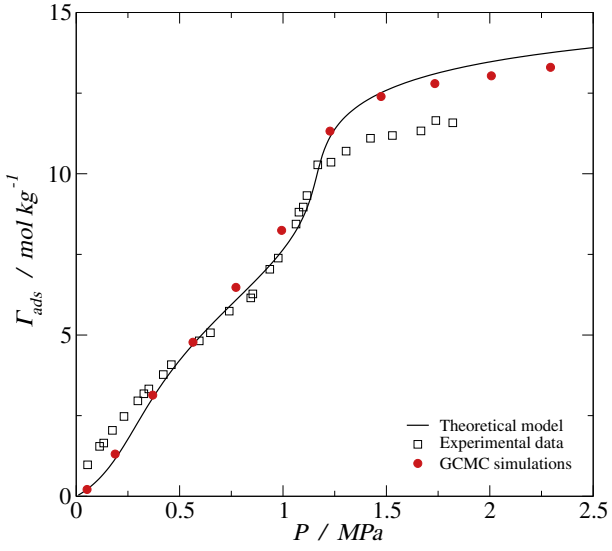

Fig. 6. Adsorption of pure ethane on MCM-41 silica at 264.75 K. Empty squares are experimental data [67], the solid line is the model from this work, and the solid circles are GCMC simulation results.

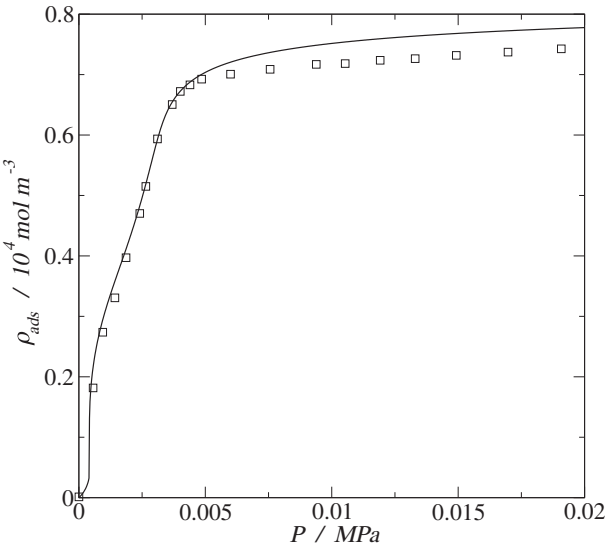

Fig. 7. Adsorption of $n-$hexane on MCM-41 at 298 K. Open squares are experimental data [68] and the solid line is the proposed model.

3.2. Ethane, $n-$hexane and benzene on MCM-41

As a case study, the adsorption of pure ethane, pure $n-$hexane and pure benzene on silica MCM-41 is analysed. The MCM-41 silica consists of hexagonally ordered arrays of long unconnected cylindrical pore channels, hence the model is well suited for this purpose.

The adsorption of ethane on a pure-silica MCM-41 sieve at 264.75 K [67] is the first set for this section. From the information reported, the porosity is 0.92 cm^3/g and the average pore diameter is 3.8 nm. The effective pore diameter used for the theoretical model is 4.2 nm, which is also used to perform Grand Canonical Monte Carlo simulations. From the adsorption of LJ fluid, we know that the potential depth of the model is around 70% of the one needed in simulation.

First, we use the experimental data to fit our model and obtain the parameters, which leads to the following values: $\epsilon_{w,\text{model}}/k = 1000$ K and $\delta_w = 0.55\sigma$. Then, we can obtain the potential depth for simulation, which is $\epsilon_{w,\text{sim}}/k = 1408$ K and a repulsive exponent for the Mie potential of $\lambda_w = 35$ (*cf.* the adsorption of the LJ fluid where $\delta_w/\sigma = 0.5$ corresponds to $\lambda_w = 40$).

Fig. 6 shows the curve predicted with our model (solid line), the experimental data (empty squares) and the GCMC simulation results (red solid circles). The agreement shown amongst the curves is of quantitative nature. Simulations and the model lead to comparable values, with both showing a small over-prediction on the liquid phase density at high pressure, suggesting heterogeneity in the experimental sample. This curve exhibits a type IV isotherm shape according to the IUPAC classification [60,17].

In order to test the proposed model for the adsorption of more complex fluids, we showcase the adsorption of $n-$hexane and benzene on MCM-41 at 298 K [68]. For MCM-41 we have that the pore volume is 0.56 cm^3/g and the pore radius is 1.52 nm, which leads to an effective pore radius of 1.745 nm.

Fig. 7 displays the adsorption of $n-$hexane, modelled in a coarse grained fashion as two tangent beads [62], on MCM-41 at 298 K. We

Table 4
Parameters for the adsorption of $n-$hexane on MCM-41.

T / K	ϵ_w/k / K	δ_w/σ
298	2350	0.70

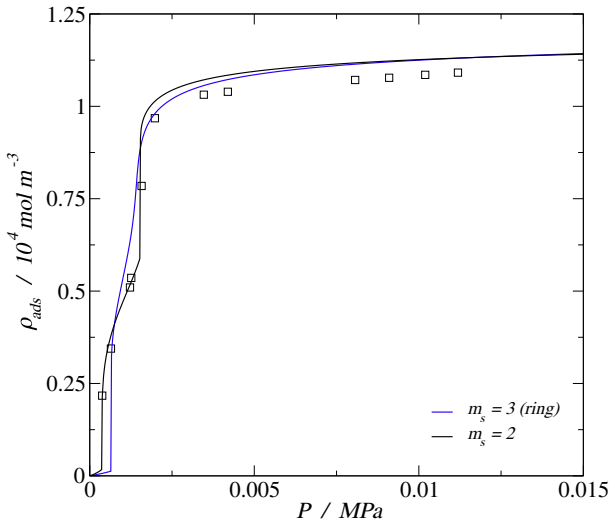

Fig. 8. Adsorption of benzene on MCM-41 at 298 K. Open squares are experimental data [68], the solid black line is the proposed model using a Coarse-Grained model of 2 beads for benzene, the solid blue line is the proposed model using a Coarse-Grained model of 3 beads (ring) for benzene.

Table 5
Parameters for the adsorption of benzene on MCM-41.

T / K	m_s	ϵ_w/k / K	δ_w/σ
298	2	2380	2170
298	3	0.70	0.90

can observe that the model predicts the adsorbed amount with good accuracy, showing a type IV isotherm for a chain molecule ($m_s = 2$) (Table 4).

The adsorption of benzene on MCM-41 at 298 K is also studied [68]. First, we use the coarse-grained model of 2 beads from Herdes et al. [62], which leads to the result showed in Fig. 8 represented by a solid black line. We can observe a good agreement between the experimental results and the molecular model using the 2-bead model for benzene.

Another set of parameters is available for benzene [64], corresponding to 3 beads in a ring-like formation (triangular configuration). To model this with the SAFT EoS, the chain term has to be changed for a ring term, which has the following form;

$$a^{\text{RING}} = (1 - m_s - \chi\eta)\ln y^M(\sigma) \tag{28}$$

where η is the packing fraction, $\eta = m_s\pi\rho\sigma^3/6$, ρ is the molecular number density, and χ is a parameter which depends on the geometry and the reference potential (for further information see ref. [64]). The latter parameter for the case of a triangular configuration is $\chi = 1.4938$.

These results are plotted in Fig. 8 alongside those of the simpler 2-bead model. Both configurations lead to similar results, showing a good agreement between the proposed model and the experimental data. Table 5 displays the parameters for the model obtained from fitting the experimental data.

3.3. Methane and carbon dioxide on shale

A further example corresponds to the adsorption of pure methane and pure carbon dioxide on mesoporous carbon [69], which can be used as surrogate models for the kerogen regions of shale rocks [70]. Fig. 9-a displays the pore size distribution (PSD) for different field samples of shales, where it is possible to observe that the main contribution is from pores with diameters between 2 and 20 nm. The average pore diameter reported is 6.8 nm, and the average porosity is 0.491 cm^3/g. To reproduce the adsorption of CH_4 and CO_2 on shale rock a mesoporous carbon is employed because, despite around 90% of the pore volume being accounted for by pores with diameters between 2 and 20 nm, it is important to consider the contributions from the other different pore sizes (Fig. 9-a). As micropores aid the adsorption in the range from low to medium pressures, they are taken into account when correlating the experimental data with the proposed model. Fig. 9-b describes a pore scheme that considers the contributions of three different pore sizes: 8% of pores with radius 0.8 nm, 87% with radius 3.4 nm, and 5% with radius 10 nm.

Considering all the pore contributions, the average adsorbed amount, Γ, and the average pore diameter, d, can be calculated from:

$$\Gamma(\rho) = \sum_i X_i\rho_i(r_{p,i}; P) \tag{29a}$$

$$d_{\text{average}} = \sum_i X_i d_i \tag{29b}$$

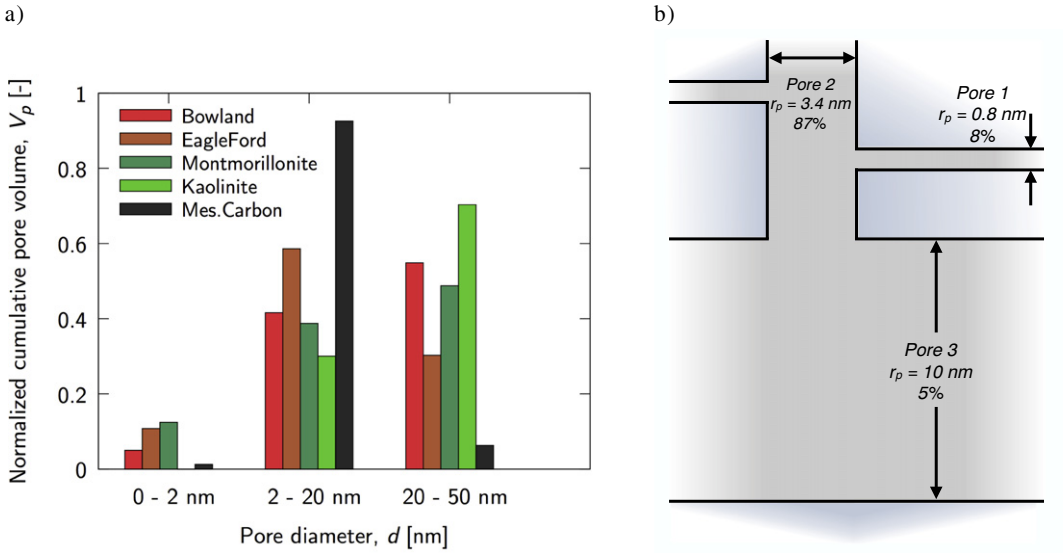

Fig. 9. a) Pore size distribution for different field sample shales [69] and the surrogate mesoporous carbon. b) Pore scheme for the mesoporous carbon.

Table 6
Parameters for the adsorption of pure methane and pure carbon dioxide on mesoporous carbon.

	Methane on mesoporous carbon				Carbon dioxide on mesoporous carbon			
T / K	$\epsilon_{w,1}/k$ / K	$\delta_{w,1}/\sigma$	$\epsilon_{w,2-3}/k$ / K	$\delta_{w,2-3}/\sigma$	$\epsilon_{w,1}/k$ / K	$\delta_{w,1}/\sigma$	$\epsilon_{w,2-3}/k$ / K	$\delta_{w,2-3}/\sigma$
313.15	950	1.5	614	0.07	1350	1.5	695	0.16
333.15	835	1.5	657	0.07	1150	1.5	715	0.16
353.15	720	1.5	700	0.07	950	1.5	735	0.16

where X_i is the percentage of each pore size in the system, ρ_i is the adsorbed density calculated from each pore size. The parameters fitted from the experimental data available are presented in Table 6, where two different sets of parameters are shown; one for methane on mesoporous carbon and the other one for carbon dioxide on mesoporous carbon. For each set we have two groups; the first one has subindex 1 that represents the smallest pore size (pore 1 in Fig. 9-b), and the second one has subindex $2-3$ corresponding to the medium and the big pore (pore 2 and 3 in Fig. 9-b). In both cases the effective wall energy of the smallest pore is much larger than those of the wider pores. This is expected, as in those ultra-confined spaces a molecule is subject to larger attractions as a consequence of the additive nature of the potential from very close walls.

Fig. 10 shows the adsorption on mesoporous carbon, where Fig. 10-a is for methane and Fig. 10-b is for carbon dioxide. The results are for three different temperatures; 313.15 K, 333.15 K and 353.15 K. The model shows a good qualitative and quantitative agreement with the experimental data, displaying type I and type IV isotherms. These results go up to 25–30 MPa, which shows that the proposed model can work in the ranges relevant to shale oil production. As expected, the adsorption of CO_2 is much more pronounced.

4. Conclusions

In this work, the SAFT-VR Mie equation of state was extended to calculate the adsorption of fluids under confinement in cylindrical nanopores. Although semi-empirical in nature, it is capable of predicting adsorption isotherms by employing two parameters related to the fluid-solid interaction; the potential depth (ϵ_w) and the range of the potential (δ_w). The proposed empirical expression for the distribution of particles inside the pore can be used with confidence to model adsorption results for complex chain fluids.

The advantage of using the SAFT equation of state is that the same molecular parameters can be used for both the bulk phase and the confined fluid properties. The proposed model is able to predict the adsorption isotherms of fluids represented by one (methane, ethane and carbon dioxide), two ($n-$hexane and benzene) and three beads (benzene and $n-$nonane), with the latter in linear and ring configuration. Removing the need to account for fluid-fluid interactions (as they are dealt with by the bulk EoS) means that the model fitting parameters account exclusively for the unknowns in the system: the intensity and range of the solid-fluid interactions. This provides for a robust and transferable set of molecular parameters along with a high-quality correlation of experimental data.

The link between the underlying physical picture and molecular simulations can be exploited to both understand and extend the potential of the model. The discussion surrounding Fig. 6 is an example of the insights that can be obtained from this simulation-theory duality. It is not possible to match perfectly the experimental data of ethane in MCM-41 to the theory for the set of data in ref. [67]. The corresponding molecular simulations, do, however, follow the theory closely. This suggests that it is our model of the surface which is failing, i.e. this particular sample may not be described as being a homogeneous cylindrical sample of a mono-disperse nanoporous radius. In a related fashion, once the adsorption curve is fitted using the theory, the molecular models can be employed in simulations to understand not only the equilibrium adsorption but the kinetics of transport through nanoporous media and other interfacial phenomena.

Acknowledgments

H.C. gratefully acknowledges the support in the form of a scholarship from CONICYT (Chile) and of the Doctoral Training on Theory and Simulation of Materials at Imperial College London funded by the U.K. Engineering and Physical Sciences Research Council (EPSRC) (EP/G036888/1). E.A.M. acknowledges the support from EPSRC through research grants to the Molecular Systems Engineering

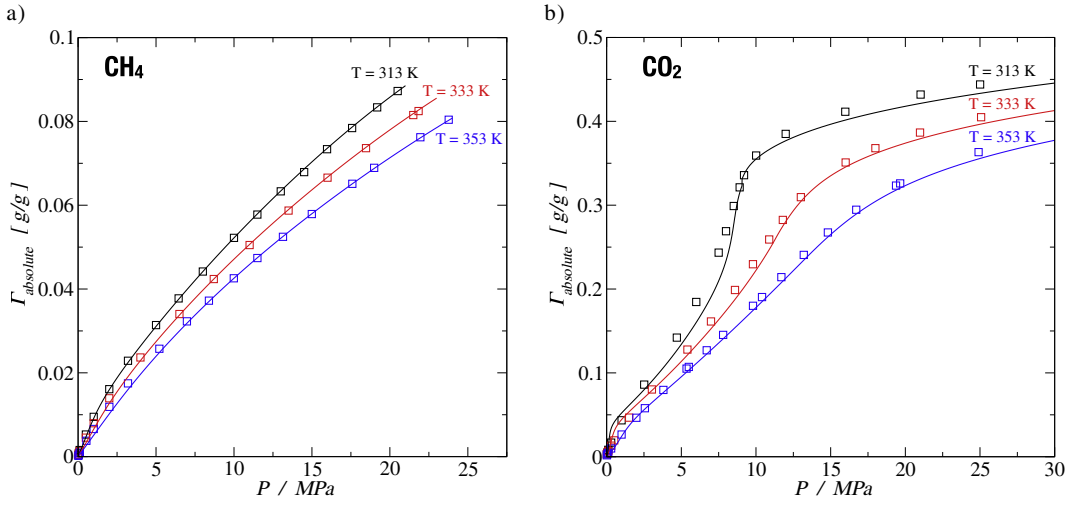

Fig. 10. Adsorption on models of shale rocks at different temperatures. a) Methane, and b) Carbon dioxide. Empty squares are experimental data [69] and the solid lines are the proposed model with parameters from Table 6.

group (grant nos. EP/E016340, EP/J014958 and EP/R013152). Computations were performed employing the resources of the Imperial College High Performance Computing Service and the UK Materials and Molecular Modelling Hub, which is partially funded by EPSRC (no. EP/P020194)

References

[1] A. Dabrowski, Adsorption - from theory to practice, Adv. Colloid Interf. Sci. 93 (2001) 135–224.
[2] E.F. Vansant, New composite adsorbents for the removal of pullants from waste waters, Stud. Surf. Sci. Catal. 120 (1998) 381–396.
[3] K. Kadirvelu, K. Thamaraiselvi, C. Namasivayam, Removal of heavy metals from industrial wastewaters by adsorption onto activated carbon prepared from an agricultural solid waste, Bioresour. Technol. 76 (2001) 63–65.
[4] Q. Liu, M. Dong, W. Zhou, M. Ayub, Y.P. Zhang, S. Huang, Improved oil recovery by adsorption-desorption in chemical flooding, J. Pet. Sci. Eng. 43 (2004) 75–86.
[5] S. Thomas, Enhanced oil recovery - an overview, Oil gas Sci. Technol. Rev. IFP 63 (2008) 9–19.
[6] N. Kabay, M. Bryjak, S. Schlosser, M. Kitis, S. Avlonitis, Z. Matejka, I. Al-Mutaz, M. Yuksel, Adsorption-membrane filtration (AMF) hybrid process for boron removal from seawater: an overview, Desalination 223 (2008) 38–48.
[7] I. Langmuir, The constitution and fundamental properties of solids and liquids, J. Am. Chem. Soc. 38 (1916) 2221–2295.
[8] H.M.F. Freundlich, Uber die adsorption in losungen, Z. Phys. Chem. 57 (1906) 385–470.
[9] S. Brunauer, P.H. Emmett, E. Teller, Adsorption of gases in multimolecular layers, J. Am. Chem. Soc. 60 (1938) 309–319.
[10] K.Y. Foo, B.H. Hameed, Insights into the modeling of adsorption isotherm systems, Chem. Eng. J. 156 (2010) 2–10.
[11] E. Kierlik, M.L. Rosinberg, Free-energy density functional for the inhomogeneous hard-sphere fluid: application to interfacial adsorption, Phys. Rev. A 42 (1990) 3382–3387.
[12] E. Kierlik, M.L. Rosinberg, Density-functional theory for inhomogeneous fluids: adsorption of binary mixtures, Phys. Rev. A 44 (1991) 5025–5037.
[13] Y.-X. Yu, J. Wu, Density functional theory for inhomogeneous mixtures of polymeric fluids, Chin. J. Chem. Phys. 117 (2002) 2368–2376.
[14] S. Tripathi, W.G. Chapman, Microstructure of inhomogeneous polyatomic mixtures from a density functional formalism for atomic mixtures, J. Chem. Phys. 122 (2005)094506–1:11.
[15] J. Liu, L. Wang, S. Xi, D. Asthagiri, W.G. Chapman, Adsorption and phase behavior of pure/mixed alkanes in nanoslit graphite pores: an iSAFT application, Langmuir 33 (2017) 11189–11202.
[16] G. Wang, J. Jiang, K. Sun, J. Wu, An improved theoretical procedure for the pore–size analysis of activated carbon by gas adsorption, Chin. J. Chem. Eng. 26 (2018) 551–559.
[17] M. Thommes, K. Kaneko, A.V. Neimark, J.P. Olivier, F. Rodriguez-Reinoso, J. Rouquerol, K.S.W. Sing, Physisorption of gases, with special reference to the evaluation of surface area and pore size distribution (IUPAC Technical Report), Pure Appl. Chem. 87 (2015) 1–19.
[18] M.M. Dubinin, The potential theory of adsorption of gases and vapors for adsorbents with energetically nonuniform surfaces, Chem. Rev. 60 (1960) 235–241.
[19] A.A. Shapiro, E.H. Stenby, Potential theory of multicomponent adsorption, J. Colloid Interface Sci. 201 (1998) 146–157.
[20] M.G. Bjørner, A.A. Shapiro, G.M. Kontogeorgis, Potential theory of adsorption for associating mixtures: possibilities and limitations, Ind. Eng. Chem. Res. 52 (2013) 2672–2684.
[21] H.K. Payne, G.A. Sturdevant, T.W. Leland, Improved two-dimensional equation of state to predict adsorption of pure and mixed hydrocarbons, Ind. Eng. Chem. Fundam. 7 (1968) 363–374.
[22] C. Zhou, F. Hall, K.A.M. Gasem, R.L.R. Jr, Predicting gas adsorption using two-dimensional equations of state, Ind. Eng. Chem. Res. 33 (1994) 1280–1289.
[23] E.A. Ustinov, D.D. Do, A. Herbst, R. Staudt, P. Harting, Modeling of gas adsorption equilibrium over a wide range of pressure: a thermodynamic approach based on equation of state, J. Colloid Interface Sci. 250 (2002) 49–62.
[24] H.Y. Zhu, L.A. Ni, G.Q. Lu, A pore-size dependent equation of state for multilayer adsorption in cylindrical mesopores, Langmuir 15 (1999) 3632–3641.
[25] G.M. Kontogeorgis, S. Kiil, Introduction to Applied Colloid and Surface Chemistry, John Wiley & Sons, New York, 2016.
[26] L. Travalloni, M. Castier, F.W. Tavares, S.I. Sandler, Thermodynamic modelling of confined fluids using an extension of the generalized van der Waals theory, Chem. Eng. Sci. 65 (2010) 3088–3099.
[27] L. Travalloni, M. Castier, F.W. Tavares, Phase equilibrium of fluids confined in porous media from an extended Peng-Robinson equation of state, Fluid Phase Equilib. 362 (2014) 335–341.
[28] G.D. Barbosa, M.L. D'Lima, S.M.H. Daghash, M. Castier, F.W. Tavares, L. Travalloni, Cubic equations of state extended to confined fluids: new mixing rules and extension to spherical pores, Chem. Eng. Sci. 184 (2018) 52–61.
[29] G.D. Barbosa, L. Travalloni, M. Castier, F.W. Tavares, Pore size distributions from extended Peng-Robinson equations of state for fluids confined in cylindrical and slit pores, Fluid Phase Equilib. 493 (2019) 67–77.
[30] W.G. Chapman, K.E. Gubbins, G. Jackson, M. Radosz, SAFT: equation-of-state solution model for associating fluids, Fluid Phase Equilib. 52 (1989) 31–38.
[31] W.G. Chapman, K.E. Gubbins, G. Jackson, M. Radosz, New reference equation of state for associating liquids, Ind. Eng. Chem. Res. 29 (1990) 1709–1721.
[32] E.A. Müller, K.E. Gubbins, Molecular-based equations of state for associating fluids: a review of SAFT and related approaches, Ind. Eng. Chem. Res. 40 (2001) 2193–2211.
[33] C. McCabe, A. Galindo, SAFT associating fluids and fluid mixtures, in: A.R.H. Goodwin, J.V. Sengers, C.J. Peters (Eds.), Applied Thermodynamics of Fluids, Royal Society of Chemistry, 2010, pp. 215–279. London.
[34] A. Martinez, M. Castro, C. McCabe, A. Gil-Villegas, Predicting adsorption isotherms using a two-dimensional statistical associating fluid theory, J. Chem. Phys. 126 (2007) 074707.
[35] J. Kern, M. Johannsen, Modeling adsorption on energetically heterogeneous surfaces with an extended SAFT-VR approach, J. Supercrit. Fluids 133 (2018) 70–76.
[36] L.F.M. Franco, I.G. Economou, M. Castier, Statistical mechanical model for adsorption coupled with SAFT-VR Mie equation of state, Langmuir 33 (2017) 11291–11298.
[37] A.Z. Panagiotopoulos, Adsorption and capillary condensation of fluids in cylindrical pores by Monte Carlo simulation in the Gibbs ensemble, Mol. Phys. 62 (1987) 701–719.
[38] S. McGrother, K.E. Gubbins, Constant pressure Gibbs ensemble Monte Carlo simulations of adsorption into narrow pores, Mol. Phys. 97 (1999) 955–965.
[39] S. Jana, J.K. Singh, S.K. Kwak, Vapor-liquid critical and interfacial properties of square-well fluids in slit pores, J. Chem. Phys. 130 (2009)214707:1–8.
[40] A. Abdelrasoul, H. Zhang, C.-H. Cheng, H. Doan, Applications of molecular simulations for separation and adsorption in zeolites, Microporous Mesoporous Mater. 242 (2017) 294–348.
[41] G.D. Barbosa, L. Travalloni, M. Castier, F.W. Tavares, Extending an equation of state to confined fluids with basis on molecular simulations, Chem. Eng. Sci. 153 (2016) 212–220.
[42] L. Kong, H. Adidharma, Adsorption of simple square-well fluids in slit nanopores: modeling based on generalized van der Waals partition function and Monte Carlo simulation, Chem. Eng. Sci. 177 (2018) 323–332.
[43] T. Lafitte, A. Apostolakou, C. Avendaño, A. Galindo, C.S. Adjiman, E.A. Müller, G. Jackson, Accurate statistical associating fluid theory for chain molecules formed from Mie segments, J. Chem. Phys. 139 (2013) 154504.
[44] T.L. Hill, An Introduction to Statistical Thermodynamics, Addison-Wesley Publishing Company, Inc.. 1980.
[45] S.I. Sandler, The generalized van der Waals partition function. I. Basic theory, Fluid Phase Equilib. 19 (1985) 233–257.
[46] D.A. McQuarrie, Statistical Mechanics, Harper & Row. 1973.
[47] G. Mie, Zur kinetischen theorie der einatomigen körper, Ann. Phys. 316 (1903) 657–697.
[48] V. Papaioannou, T. Lafitte, C. Avendaño, C.S. Adjiman, G. Jackson, E.A. Müller, A. Galindo, Group contribution methodology based on the statistical associating fluid theory for heteronuclear molecules formed from Mie segments, J. Chem. Phys. 140 (2014) 1–29. 054107.
[49] J.M. Prausnitz, R.N. Lichtenthaler, E.G. de Azevedo, Molecular Thermodynamics of Fluid-phase Equilibria, third ed., Prentice-Hall. 1999.
[50] G.E. Mueller, Numerically packing spheres in cylinders, Powder Technol. 159 (2005) 105–110.
[51] E. Santiso, E.A. Müller, Dense packing of binary and polydisperse hard spheres, Mol. Phys. 100 (2002) 2461–2469.
[52] D. Frenkel, B. Smit, Understanding Molecular Simulation: From Algorithms to Applications, Academic Press, London, 2002.
[53] D. van der Spoel, E. Lindahl, B. Hess, G. Groenhof, A.E. Mark, H.J. Berendsen, GROMACS: fast, flexible and free, J. Comput. Chem. 26 (2005) 1701–1718.
[54] Y. Kadiri, R. Albaki, J.L. Bretonnet, Thermodynamic equivalence between the Lennard-Jones and hard-core attractive Yukawa systems, Chem. Phys. 352 (2008) 135–141.
[55] J. Jover, A.J. Haslam, A. Galindo, G. Jackson, E.A. Müller, Pseudo hard-sphere potential for use in continuous molecular-dynamics simulation of spherical and chain molecules, J. Chem. Phys. 137 (144505) (2012) 1–13.
[56] N.S. Ramrattan, C. Avendaño, E.A. Müller, A. Galindo, A corresponding-states framework for the description of the Mie family of intermolecular potentials, Mol. Phys. 113 (2015) 932–947.
[57] E. Forte, A.J. Haslam, G. Jackson, E.A. Müller, Effective coarse-grained solid-fluid potentials and their application to model adsorption of fluids on heterogeneous surfaces, Phys. Chem. Chem. Phys. 16 (2014) 19165–19180.
[58] H.C. Hamaker, The London-van der Waals attraction between spherical particles, Phys. IV 10 (1937) 1058–1072.
[59] G. Jiménez-Serratos, H. Cárdenas, E.A. Müller, Extension of the effective solid-fluid Steele potential for Mie force fields, Fluid Phase Equilib. (2019) (in press).
[60] S. Brunauer, L.S. Deming, W.E. Deming, E. Teller, On a theory of the van der Waals adsorption of gases, J. Am. Chem. Soc. 62 (1940) 1723–1732.
[61] S. Dufal, T. Lafitte, A.J. Haslam, A. Galindo, G.N.I. Clark, C. Vega, G. Jackson, The A in SAFT: developing the contribution of association to the Helmholtz free energy within a Wertheim TPT1 treatment of generic Mie fluids, Mol. Phys. 113 (2015) 948–984.
[62] C. Herdes, T.S. Totton, E.A. Müller, Coarse grained force field for the molecular simulation of natural gases and condensates, Fluid Phase Equilib. 406 (2015) 91–100.
[63] C. Avendaño, T. Lafitte, A. Galindo, C.S. Adjiman, G. Jackson, E.A. Müller, SAFT-γ force field for the simulation of molecular fluids. 1. A single-site coarse grained model of Carbon Dioxide, J. Phys. Chem. B 115 (2011) 11154–11169.

[64] E.A. Müller, A. Mejía, Extension of the SAFT-VR Mie EoS to model homonuclear rings and its parametrization based on the principle of corresponding states, Langmuir 33 (2017) 11518–11529.
[65] Q. Wu, L. Zhou, J. Wu, Y. Zhou, Adsorption equilibrium of the mixture $CH_4+N_2+H_2$ on activated carbon, J. Chem. Eng. Data 50 (2005) 635–642.
[66] A.J. Fletcher, K.M. Thomas, Adsorption and desoprtion kinetics of *n*−octane and *n*−nonane vapors on activated carbon, Langmuir 15 (1999) 6908–6914.
[67] J.-H. Yun, T. Düren, F.J. Keil, N.A. Seaton, Adsorption of methane, ethane, and their binary mixtures on MCM-41: experimental evaluation of methods for the prediction of adsorption equilibrium, Langmuir 18 (2002) 2693–2701.
[68] M.M.L.R. Carrott, A.J.E. Candeias, P.J.M. Carrott, P.I. Ravikovitch, A.V. Neimark, A.D. Sequeira, Adsorption of nitrogen, neopentane, *n*−hexane, benzene and methanol for the evaluation of pore sizes in silica grades of MCM-41, Microporous Mesoporous Mater. 47 (2001) 323–337.
[69] R. Pini, Adsorption of CH_4 and CO_2 on mesoporous carbon at different temperatures, 2019. unpublished.
[70] C. Herdes, C. Petit, A. Mejía, E.A. Müller, Combined experimental, theoretical, and molecular simulation approach for the description of the fluid-phase behavior of hydrocarbon mixtures within shale rocks, Energy Fuel 32 (2018) 5750–5762.